Risk Analysis of Hazardous Events in Stochastic System via Markov Chain Estimation using Monte Carlo

Ludwig Horvath
ludhor@kth.se

Lucille Huriez
huriez@kth.se

Oliver Ribohn
oribohn@kth.se

Cornelia Sparring
corspa@kth.se

Linnéa Östlund
lostl@kth.se

October 2024

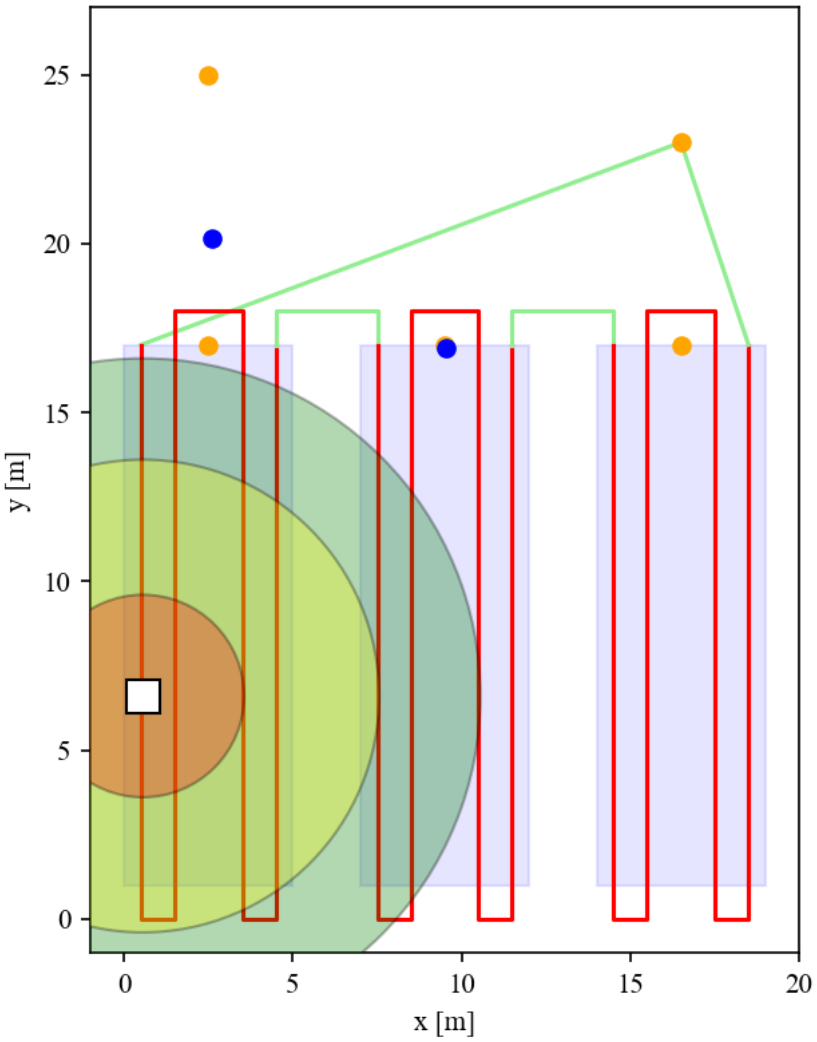

Figure 1: Screenshot of the animation produced by the simulation software.

Abstract

This report aims to analyze the risk of human injury due to UV-C light exposure during the operation of an autonomous robot in strawberry cultivation. The study employs the Monte Carlo method to estimate a Markov Chain, modeling the system's dynamics. Simulations are conducted in a customized environment that accounts for human movement, sensor accuracy, and robot behavior. This environment facilitates a comprehensive analysis by calculating the system's transition matrix, absorption probabilities, and conducting sensitivity analysis.

The software allows for a high degree of modularity, enabling users to easily modify various parameters to adapt the risk analysis to different facilities or scenarios. Beyond its calculative capabilities, the simulation environment enhances the user experience by offering a structured approach to analysis. All results are saved in an organized folder system, and users can record and save videos of outcomes of interest, see screenshot of simulation in figure 1. The environment also supports automated generation of results across a parameter space and fits a model to the risk hyperplane using kernel regression, a capability which is utilized in the results and discussion section of this report.

The analysis compares two sensor types: a standard RGB-D camera and a higher-quality RGB-D camera with LiDAR. Additionally, it examines human risk responses based on varying levels of training. By simulating different scenarios, the probability of injury is calculated for both trained and untrained individuals with each sensor. This analysis highlights how sensor performance and human response influence the overall risk of injury.

Contents

1 Introduction

Recent advancements in sensing, machine learning and actuation have enabled robotic autonomous systems to play an increasingly significant role in the agricultural sector. These technologies are transforming traditional farming methods, allowing tasks to be performed with greater precision, efficiency, and sustainability. One particular application involves the use of autonomous robots to perform UV light treatments on plants in controlled environments. [4] [5]

This project, assigned by NMBU, focuses on a system specifically designed for strawberry fields located inside polytunnels. The robot autonomously navigates the rows of plants while using UV-C light to treat the berries, leading to a significant reduction in the need of fungicide application. While this technique is highly beneficial for plant health, it also poses a risk to humans entering the fields during the treatment process, as UV-C light exposure can cause severe eye damage. The risk arises when humans approach the robot while it is active, particularly within a critical distance of three meters or less. The robot is equipped with a sensor system designed to detect the presence of people at various distances, enabling it to issue audiovisual alerts or stop its operation if necessary. However, failures in the system, such as the inability to detect a person at the correct distance, can lead to hazardous situations. [3]

The aim of the project is to develop a probabilistic model that can estimate the likelihood of human injury caused by the UV light for people who interact with the robot. This involves modeling human behaviour, sensor accuracy and robot movement as concurrent modules.

The main research question to be answered is:

What is the probability of injury caused by UV-light from the autonomous agriculture robot and how does it relate to different parameters of the system?

When investigating this research question, especially in terms of the defining parameters of the system, a focus is dedicated towards variation in:

1. Human presence, specifically in terms of the number of visitors and workers in the environment.
2. Sensor detection accuracy, denoted as P_f, which refers to the probability of a sensor failing to detect hazards (false negatives).
3. Standard deviation of measurements in working region σ, particularly the standard deviation of the normal distributed unbiased case of the measurement.

2 Method

The aim is to calculate the risk of injury, which occurs when a person is within 3 meters of the robot while its UV-light is activated. This requires accounting for several non-deterministic factors, such as sensor capabilities and human behavior. To model these uncertainties, the environment, human behavior, robot movements and sensor performance will be represented by using a Markov chain. To determine the probabilities of transitioning between states, a a large number of iterations will be made to generate a transition matrix. The resulting matrix will then be used to calculate the probability of an injury occurring. This approach, known as a Monte Carlo simulation, relies on random sampling and repeated trials to estimate outcomes in systems with uncertainty.

2.1 State space formulation

Four critical limits are defined in terms of the distance from the robot to the closest human. Their criticality of the borders stem from the possible implication when crossing them. Distances in between critical ones are grouped together, thus eliminating the need for a continuous description.

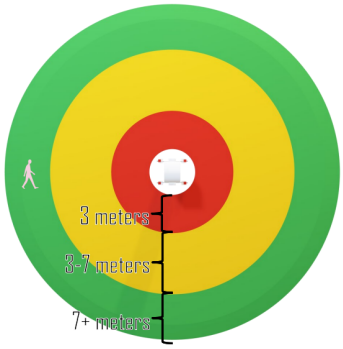

Figure 2: The different zones where the sensor can detect humans.

It was deemed that one appropriate way to define that state space was by the following state variables.

$$\begin{aligned} m \in \mathcal{M} \qquad & \mathcal{M} = \{0, 1\} \\ u \in \mathcal{U} \qquad & \mathcal{U} = \{0, 1\} \\ d \in \mathcal{D}^* \qquad & \mathcal{D}^* = \{3, 7, 10, 100\} \\ d^* \in \mathcal{D} \qquad & \mathcal{D} = \{3, 7, 10, 100\} \end{aligned}$$

A few key definitions can now be introduced:

- $m \in \mathcal{M}$: The *mode* of the robot, where $m = 1$ and $m = 0$ represents if the robot is operating or not, respectively.
- $u \in \mathcal{U}$: The binary state of the UV-light, where $u = 1$ and $u = 0$ represents the UV-light being on or off, respectively.
- $d^* \in \mathcal{D}^*$: The estimated least upper bound of the distance to the closest person based on sensor data.
- $d \in \mathcal{D}$: The true least upper bound of the distance to the closest person.

The states describing the characteristics of the robot, as well as its relationship to the humans can be described as all possible combination of elements from these sets,

$$s \in \mathcal{S} := \mathcal{M} \times \mathcal{U} \times \mathcal{D}^* \times \mathcal{D}$$

where $s \in \{1, 2, \ldots, |S|\}$.

2.1.1 Absorbing states

Additionally, two absorbing states which each represent disjoint events from any other state will be added to the model, representing the events of injury and reaching goal. The size of the discrete state space is thus

$$|\mathcal{S}| = 2 \cdot 2 \cdot 4 \cdot 4 + 2 = 66$$

different states, where s_{65} is the *goal state* and s_{66} the *injury state*. Upon entering one of the two absorbing states, the simulation will stop.

2.1.2 Inaccessible states

A subset of the state space are by logic neither transient nor absorbing - as their are inaccessible. This due to them being impossible events. Consider for instance the event $\{m = 0, u = 1\}$ which, for reasons that will be clarified, can never be reached.

2.1.3 Transient states

For any accessible state which is not an absorbing state, is guaranteed to be a transient state as it communicates with an absorbing state. Any state in the state space, which is not explicitly stated to be absorbing nor inaccessible, can be assumed to be a transient state.

2.1.4 Encoding the states

To effectively store, represent and target states it is helpful to consider how they are to be encoded. This also implies constant time complexity, whenever an algorithm is to fetch the value of a certain state.

Consider the non-absorbing state space $\mathcal{M} \times \mathcal{U} \times \mathcal{D}^* \times \mathcal{D}$. Each state variable can assume a number of different values, hence a set can be defined as

$$s = (m_i, u_j, d_k^*, d_l)$$

where the indices correspond to the following:

$$i_m \in \{0, 1\} \text{ where } i_m : m_i \in \mathcal{M} \qquad i_u \in \{0, 1\} \text{ where } i_u : u_j \in \mathcal{U}$$
$$i_{d^*} \in \{0, 1, 2, 3\} \text{ where } i_d : d_k^* \in \mathcal{D}^* \qquad i_d \in \{0, 1, 2, 3\} \text{ where } i_l : d_l \in \mathcal{D}$$

The index (i, j) of a transition probability in the soon to be introduced transition matrix $P := [p_{i,j}]$ can thus be calculated by

$$i = 32 \cdot i_m + 16 \cdot i_u + 4 \cdot i_{d^*} + 4 \cdot i_d, \quad i \in \{0, 1, 2, \ldots, 63\} \tag{1}$$

The indices of absorbing states are given explicitly as

$$i_G = 64 \qquad i_I = 65$$

Illustration in figure 3 showcases the mapping of the different states onto a linear structure of 66 dells.

Figure 3: Mapping of multi-dimensional transient state space to a linear structure with 64 cells.

2.2 Estimating Transition Probabilites

One objective, to obtain a stochastic model of the system, is to obtain the Markov chain. As the state space is defined, what remains it to determine the probabilities of transitioning between each state pair

$$p_{i,j} := \mathbb{P}(s_{t+1} = j, s_t = i) \quad \forall \quad (i,j) \in \{1, \dots, |\mathcal{S}|\}^2 \tag{2}$$

The transition matrix, denoted P, is defined as

$$P := [p_{i,j}] \quad \forall \quad (i,j) \in \{1, \dots, |\mathcal{S}|\}^2 \tag{3}$$

The event space of interest here is the following σ-algebra

$$\mathcal{F} := \{(i,j)\} = \mathcal{S} \times \mathcal{S}$$

As $\mathcal{F}$ defines a σ-algebra, it can be stated that

$$p_{i,j} := \mathbb{P}(s_{t+1} = j, s_t = i) = \mathbb{E}\left[\mathbb{1}_{i,j}\right] \tag{4}$$

Let σ-algebra be constructed from the events representing the set of possible sequences produced from the Markov chain, each appended sequence terminates at an absorbing state. Mathematically, this can be represented as the set

$$\{((i,j)_{1,1}, \dots, (i,j)_{n_1,1}), ((i,j)_{2,2}, \dots, (i,j)_{n_2,2}), \dots ((i,j)_{1,N}, \dots, (i,j)_{n_N,N})\}$$

where $(i,j)_{n_k,k}$ is the active state at n_k during the k:th simulation. Each sequence is a sample from the same Markov chain, which is invariant over the variable k, indicating the number of the simulation being nothing but a label. It is therefore assumed that each sample is *i.i.d.* Assuming *ergodicity* of $\mathbb{1}_{(i,j)_{n_k,k}}$ in k. The *weak law of large numbers* states that

$$\frac{1}{n} \sum_{k=1}^{n} \mathbb{1}_{(i,j)_{n_k,k}} \xrightarrow{P} \mathbb{E}\left[\mathbb{1}_{i,j}\right] \text{ as } N \to \infty \tag{5}$$

Thus, using the l.h.s. of (5) and (4), one can in theory acquire the true transition probabilities $p_{i,j}$ for all (i,j) in $\mathcal{F}$. Then by (3), one can thus acquire the transition matrix P. The steps are efficiently conveyed in an algorithm as below.

Algorithm 1 Estimating the Transition Matrix P

1: **Input**: Number of simulations N, state space $\mathcal{S}$
2: **Initialize**: Transition count matrix $C \in \mathbb{R}^{|\mathcal{S}| \times |\mathcal{S}|}$, initialized to zero
3: **for** each simulation $k = 1$ to N **do**
4: **while** Markov chain has not terminated **do**
5: Observe transition $(i \to j)$
6: Increment the count $C(i,j)$ by 1
7: **end while**
8: **end for**
9: Compute the transition probabilities:

$$p_{i,j} = \frac{C(i,j)}{\sum_j C(i,j)} \quad \forall \quad (i,j) \in \mathcal{S} \times \mathcal{S}$$

10: Construct the transition matrix:

$$P = [p_{i,j}] \quad \forall \quad (i,j) \in \mathcal{S} \times \mathcal{S}$$

11: **Output**: Transition matrix P

2.3 Estimating Absorption Probabilities

The main goal is to estimate risk. The risk is the relative frequency of the absorbing state i_G occurring. For irreducible Markov chains the steady state probabilities are often of major interest, but for a Markov chain with absorbing states as in this case, it is rather the probabilities of absorption.

Consider representing the probability of absorption in state i, starting from state j, as

$$f_{ij} = \mathbb{P}(\text{absorption in state } i \mid \text{starting in state } j).$$

If i is an absorbing state, then the probability of absorption is trivial:

$$f_{ii} = 1 \quad \text{for any absorbing state } i.$$

For transient states i, the absorption probability f_{ij} can be expressed using first-step analysis. Consider that in one step, the chain may move to some state k with probability p_{ik}, and from there, it will be absorbed into j with probability f_{kj}. Deduced from this one can write the following equation for f_{ij}:

$$f_{ij} = \sum_k p_{ik} f_{kj}$$

where the sum is taken over all possible states k. Let i be a transient state, and for every j (an absorbing state), the former equation can be split into two parts:

$$f_{ij} = \sum_{k \in \text{transient}} p_{ik} f_{kj} + \sum_{k \in \text{absorbing}} p_{ik} f_{kj}$$

As $f_{kj} = 1$ for absorbing states $k = j$, equation simplifies to:

$$f_{ij} = \sum_{k \in \text{transient}} p_{ik} f_{kj} + p_{ij}$$

To solve the system of equations, the system is expressed in matrix form. Suppose the transition matrix P is known, then it can be partitioned in the following way

$$P = \begin{pmatrix} Q & R \\ 0 & I \end{pmatrix}$$

where Q represents the transition probabilities between transient states, R represents the transition probabilities from transient to absorbing states, I is the identity matrix for the absorbing states, and the 0 block represents no transitions from absorbing to transient states. The system of equations for the absorption probabilities can then be written as:

$$f = Qf + R$$

which clearly aligns with the former result in component form. By rearranging the equation $f = Qf + R$ and solving for f, we get:

$$f = (I - Q)^{-1} R$$

This produces the absorption probabilities matrix f for all transient states.

There is the possibility that the transition matrix P ends up having 0 rows and columns, this implies the existence of inaccessible states. It can either be identified from the logic of the state space, certain transitions are easy to identify as having 0 probability. Another way is to do a lot of simulations, and noticing that it never results in non-zero values in certain elements. One remedy to this situation is to exclude these rows and columns from the Q matrix, let Q' be the matrix with redundancy and Q be the matrix with no inaccessible states. The same calculation can be performed, obviously the absorption probabilities will apply to all states except for the excluded inaccessible ones which will have a zero probability of ending up in an absorbing state.

3 Models

In order to simulate the behavior of the robot, humans, and the surrounding environment, several key assumptions must be made. These assumptions influence how different agents interact within the environment. Each assumption leads to a specific model that characterizes the robot, humans, and the environment, shaping the dynamics of the simulation. Below is an outline of these models and their implications. Each subsection focuses starts with the assumptions, then moves on to mathematical formulations and details regarding implementation.

3.0.1 Model of Environment

The model will include three 5×25 meter large fields covered by polytunnels, with four rows of strawberries in each field. There is one entrance located at the upper left corner of the facility. A charging station for the robot is situated in the upper right corner, where the robot, depending on the battery level, either recharges or is stored after completing a full run through the 12 rows.

Figure 4 provides a sketch of the environment. The orange lines represent the possible paths of the humans between the five points $z_1 = (2.5, 26)$, $z_2 = (2.5, 16)$, $z_3 = (9.5, 16)$, $z_4 = (16.5, 16)$ and $z_5 = (16.5, 24)$. The first point, z_1, represents the facility entrance and is of interest since people must enter from some direction. Points z_2, z_3 and z_4 are located at one field each, in an area where hazardous events may occur. The last point, z_5, corresponds to the charging station, where people may go for doing maintenance etc.

The path of the robot is predetermined. The green lines represent the robot's path when it is not operating. This includes the movement outside the fields when the UV-light is off, i.e., during field transitions and movement to and from the charging station. In contrast, red lines correspond to the robot's path outside the fields while it is still operating, i.e., during row transitions. Thus, the red lines surrounding z_2, z_3 and z_4 define the areas of potential risk. If the robot successfully returns to the charging station without any injury, the model reaches the absorbing state representing goal.

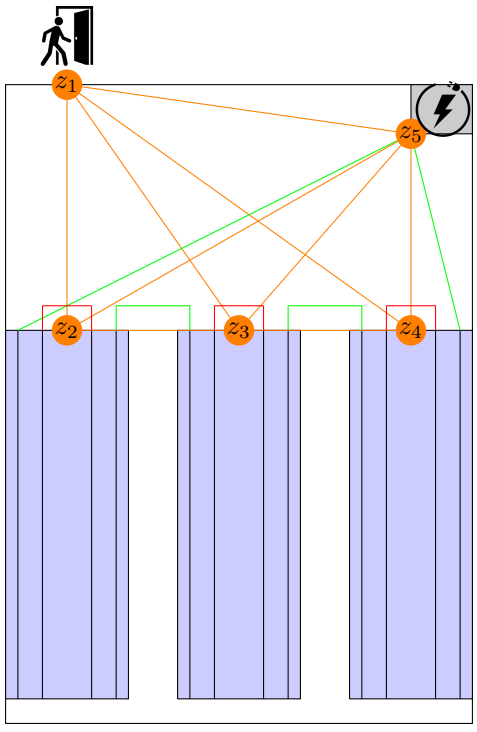

Figure 4: Sketch of the environment and the paths of humans and robot.

3.0.2 Model of Robot

The robot is confined to linear movement in the horizontal plane. It has, as any robot, a built in state space machine. But since it much accommodate for the dynamic environment it can't solely rely on deterministic behaviour. There are thus fallback protocols in the state-machine which are governed by stochastic outcomes. In this study, the main stochastic element from the robots view is the detection of humans within the critical zones.

Assumptions:

1. **Linear movement constraint**: The robot is restricted to moving only in straight lines in the horizontal plane, limiting its flexibility in adapting to dynamic environments.
2. **Stochastic fallback protocols**: The robot's state machine, though primarily deterministic, relies on stochastic protocols for human detection. This introduces randomness in its behavior, reducing predictability in safety-critical situations.
3. **Fixed human detection range**: The robot's behavior is based on detecting humans within a predefined range (7–10 meters). This fixed threshold may not adequately account for variations in human speed, direction, or unexpected obstacles, limiting its real-world applicability.

The intended goal of the robot is to go from the charging station, across the rows in each field to treat all the plants, and then go back to the charging station. However, human movement might interfere, since the robot will pause if a human is detected nearby. To account for these potential interference's and adjust the robot's behavior accordingly, the subsystem of the robot includes different states and characteristics that help manage the robot's interactions with humans. The flowchart in figure 5 provides a clearer illustration of the behavior of the robot based on the sensor's measurements in each time step. Alarm is abbreviated by "a" and UV by "u", the values assume 1 or 0 depending whether alarm or UV is on or not.

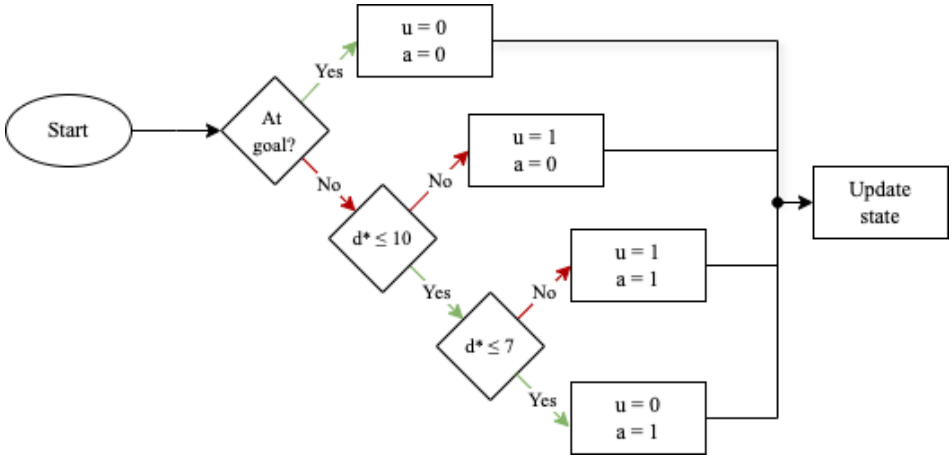

Figure 5: Flowchart illustrating the robot's behaviour in each time step when it is operating

If the robot has reached its goal, i.e., back at the charging station without any injury occurring along the path, it stops and the UV-light turns off. It has then fulfilled one iteration of the simulation without any dangerous events occurring. If the robot has not yet reached the charging station, it uses its sensors to detect nearby humans. If no human is detected within 10 meters, the robot continues its path without any alarm or intervention. If a human is detected between 7 and 10 meters away, the robot proceeds with the alarm activated. In the case a human is detected within 7 meters, there is a risk of injury, so the robot stops, turns off the UV-light if it is operating, while the alarm remains on. Another reason to why the UV-light is deactivated when the robot stands still is to prevent overexposure that could damage the crops.

3.0.3 Model of Detection System

There are two different types of detection systems considered:

1. RGB-D + CNN: RGB-D camera utilizing CNN technology
2. RGB-D + LiDAR: RGB-D camera + 3D LiDAR

Assmptions:

1. **Detection Through Material:** Both sensors are assumed to effectively detect people through the material of the polytunnels, ensuring accurate alarm activation for upcoming row transitions.
2. **Measurement Error:** The sensors may experience local measurement errors, leading to discrepancies between detected distances and actual true distances.
3. **Unexpected Objects:** The presence of unexpected objects in the environment may affect sensor readings, potentially leading to incorrect detections.
4. **Random Measurements:** The sensors may encounter random measurements, which can include phantom readings or interference from other sources.
5. **Environmental Interference:** Sensor performance may be compromised due to environmental factors, such as bright sunlight or specular reflections, which can lead to failures in detection.

Table 1: Summary of Sensor Performance Cases

Case Notation	**Event Description**	**Distribution**
C_1	Random Measurements but Detected	Uniform Distribution
C_2	Unbiased Measurement	Normal Distribution
C_3	Failure due to Environmental Interference	Probability = 1 (sensor reads > 10 m)

The probability of a sampled distance d^* conditioned on the true distnace d is $\mathbb{P}(d^* \mid d)$, which can be expanded using the law of total probability as

$$\mathbb{P}(d^* \mid d) = \mathbb{P}(d^* \mid C_1, d)\mathbb{P}(C_1) + \mathbb{P}(d^* \mid C_2, d)\mathbb{P}(C_2) + \mathbb{P}(d^* \mid C_3, d)\mathbb{P}(C_3) \tag{6}$$

- C_1 implies PDF f_1:

$$f_1(d^*) = \frac{1}{10} \cdot \mathbb{1}_{\{0 \leq d^* \leq 10\}} \tag{7}$$

- C_2 implies PDF f_2:

$$f_2(d^*) = \frac{1}{\sigma\sqrt{2\pi}} e^{-\frac{(d-d^*)^2}{2\sigma^2}} \cdot \mathbb{1}_{\{d \in \mathbb{R}\}} \tag{8}$$

- C_3 implies PDF f_3:

$$f_3(d^*) = \mathbb{1}_{\{d^* = 100\}} \tag{9}$$

Using the law of total probability, (6), (7), (8) and (9) the following result is obtained.

$$f(d^*) = f_1\mathbb{P}(C_1) + f_2(d^*)\mathbb{P}(C_2) + f_3(d^*)\mathbb{P}(C_3)$$

Choosing $\mathbb{P}(C_1)$, $\mathbb{P}(C_2)$, and $\mathbb{P}(C_3)$ such that they sum to 1 will ensure that the PDF integrates approximately to 1. The characteristics of the probability density function and the categorization of the different cases are based on a model motivated by Sebastian Thrun in section 6.3 of *Probabilistic Robotics*.[6]

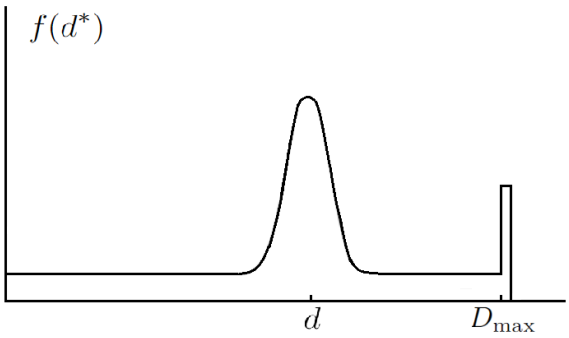

Figure 6: Illustration of the PDF for sensor performance.

The sensor measurement includes unbiased noise, represented by the standard deviation σ, which is a defining parameter of f_2. The value of σ will differ between the two sensors, since the high-quality sensor has better precision than the standard sensor. The parameters λ_i, $i = 1, 2, 3$, are scaling factors that adjust the influence of each component of the PDF. These depend on the accuracy of the sensor, and will thereby also differ between the two sensors. The selected parameter values are given in table 2, and are based on specifications found in [1] and [2].

Parameter	Standard Sensor	High-Quality Sensor
σ	$0.02d$	$0.01d$
$\lambda_1 := \mathbb{P}(C_1)$	ϵ	ϵ
$\lambda_2 := \mathbb{P}(C_2)$	$0.9993 - \epsilon$	$0.9994 - \epsilon$
$\lambda_3 := \mathbb{P}(C_3)$	0.0007	0.0006

Table 2: Values of the parameters used to model the sensor.

The idea of this model is to capture important failure-related phenomena that is associated with typical sensor fusion methodologies. At the same time the model is parameterized in just a few parameters: λ_1, λ_2, λ_3 and σ. In case of implementation, one could possibly fit the true probability distribution to the proposed mode by using the following methodology.

Steps to Fit the True System PDF to the Model

1. **Collect Data:**
   - Gather input and output data from the sensor system.
2. **Classify Data:**
   - Sort measurements into three categories: C_1, C_2, or C_3.
3. **Estimate Variance σ for C_2:**
   - Use regression (e.g., kernel regression) on the C_2 data to model the normal distribution.
   - Estimate the variance σ using i.e. rejection sampling.
4. **Assemble the Model:**
   - Combine the estimated parameters λ_1, λ_2, λ_3, and σ into the model.
5. **Test the Model:**
   - Validate the model by testing it against real data or using simulation software.

3.0.4 Model of human behaviour

The simulation includes two types of persons: *trained* workers and *untrained* visitors. Since workers and visitors are assumed to have different purposes, their movement patterns are expected to differ. Furthermore, since visitors are less aware of potential hazards, their likelihood of being injured is deemed higher, mainly due to lack of training and experience. Workers and visitors both move at a constant speed of 5 km/h, assuming they are not reacting to any alerts.

The subsystem representing the human movement will be modelled as stochastic movement between the set-points z_i, $i = 1, ..., 5$, by using a Markov chain. Different transition matrices will be used for workers and visitors, where each element represents the probability of moving from one set-point to another. To account for the probability of a person remaining at specific points, higher values are assigned to the diagonal elements of the matrices. This reflects the increased likelihood of staying at the same point compared to transitioning to another point. The transition probabilities, p_{ii}, will be estimated by making assumptions about the dwell times T_i, which represent the expected number of time steps that an individual remains in state z_i before transitioning to another state. The dwell times are related to the diagonal elements of the transition matrix according to equation 10.

$$T_i = \frac{1}{1 - p_{ii}} \iff p_{ii} = 1 - \frac{1}{T_i} \tag{10}$$

The time step at which the worker leaves state z_i can be seen as a random variable following a geometric distribution with parameter $1 - p_{ii}$. The dwell time represents the expected value of this variable, which clarifies the relationship in equation 10. The assumed expected dwell times, $T^{(\mathrm{w})}$ for workers and $T^{(\mathrm{v})}$ for visitors, for each setpoint can be seen in table 3. These are given in seconds since in the simulation, one time step corresponds to one second. The values of the dwell times are based on reasonable assumptions. At the entrance, workers are not assumed to have any specific intentions, this dwell time is set to 0. Workers, however, may spend some time at the entrance observing the fields, resulting in a dwell time of 5 seconds. It is assumed that workers have more purpose and assignments at the fields compared to visitors, who are primarily there to observe, which motivates the longer dwell times for workers in these states. Additionally, a larger dwell time is assigned at the charging station for workers than for visitors, to represent work such as maintenance.

z_i	$T_i^{(\mathrm{w})}$	$T_i^{(\mathrm{v})}$
z_1	0	5
z_2	30	20
z_3	30	20
z_4	30	20
z_5	30	15

Table 3: Expected dwell times $T^{(\mathrm{w})}$ for workers and $T^{(\mathrm{v})}$ for visitors in the different states.

After obtaining the diagonal elements of the transition matrices, the remaining elements has to be determined. This was done by assuming that the workers mostly move towards the fields from left to right from the entrance, before proceeding to the charging station. In contrast, visitors are assumed to first examine the charging station before moving towards the fields. The assumptions on dwell times and paths resulted in the transition matrices $P^{(\mathrm{w})}$ for workers and $P^{(\mathrm{v})}$ visitors.

$$P^{(\mathrm{w})} = \begin{bmatrix} 0 & 0.1 & 0.1 & 0.1 & 0.7 \\ 0.003 & 0.97 & 0.006 & 0 & 0.021 \\ 0.0015 & 0.0225 & 0.97 & 0.003 & 0.003 \\ 0.0015 & 0 & 0.024 & 0.97 & 0.0045 \\ 0.006 & 0.003 & 0.003 & 0.018 & 0.97 \end{bmatrix} \quad P^{(\mathrm{v})} = \begin{bmatrix} 0.8 & 0.07 & 0.05 & 0.04 & 0.04 \\ 0.005 & 0.95 & 0.025 & 0 & 0.02 \\ 0.0075 & 0 & 0.95 & 0.02 & 0.0225 \\ 0.01 & 0 & 0.005 & 0.95 & 0.035 \\ 0.035 & 0.014 & 0.007 & 0.014 & 0.93 \end{bmatrix}$$

The number of workers and visitors in the model is specified before starting a simulation. In the beginning of each iteration and for each human, two points z_i and z_j, $i, j \in \{1, .., 5\}$, $i \neq j$, are randomly generated. The starting position of the human is uniformly distributed along the line connecting these two points, and the initial walking direction is from z_i towards z_j. At each time step, the human's position is updated. Additionally, both the actual distance between the human and the robot, d, and the distance measured by the sensor, d^*, are checked. If $d = 3$ and $u = 1$, an injury has occurred and the simulation stops. If $d > 3$, the next step is to check whether $d^* = 100$, in which case the human continues walking towards the goal. Conversely, if the human reacts when $d^* \leq 10$, i.e., when the alarm is on, the human moves away from the robot with increased speed. A flowchart describing the human model can be found in figure 7.

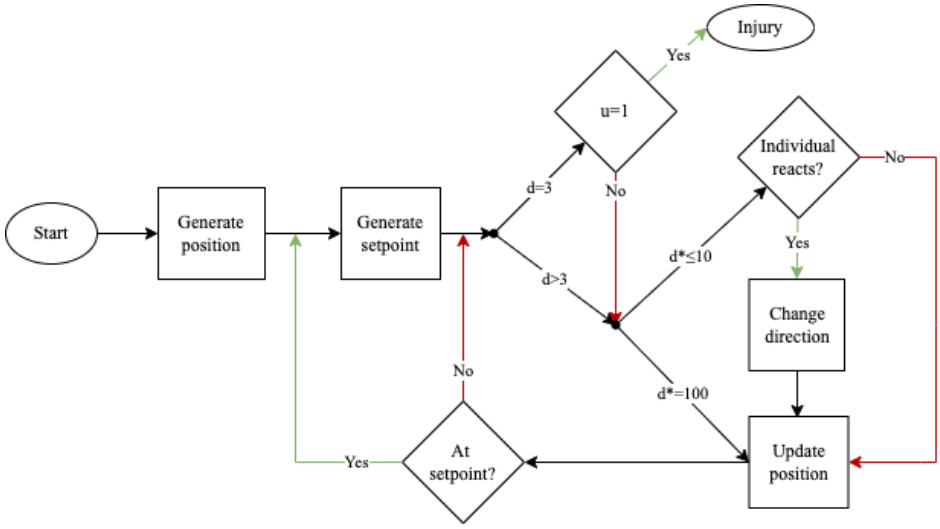

Figure 7: Flowchart of one time step in the human model.

The human response to the alarm is modelled by analyzing the relationship between the movement directions of the human and robot when they get close. To model the human reaction, some definitions are introduced:

- Leaving point z_i: point that the human walks from
- Chasing point z_j: point that the human walks towards
- Direction $\vec{z}_{ij}$: the vector from z_i to z_j

Human velocity is modelled as a combination of a nominal velocity and a reactive velocity. The nominal is entirely dependent upon the current set-point and position of the human agent, while the reactive behaviour stems from its relation to the robot in terms their relative position and velocity. The situation is illustrated in figure 8.

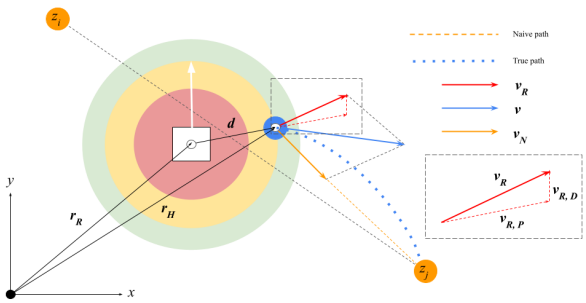

Figure 8: Diagram illustrating the activation function scale(d)

The nominal velocity of the human, $\vec{v}_N$, is defined as

$$\vec{v}_N = \frac{\vec{z}_{ij}}{||\vec{z}_{ij}||} v_N,$$

where v_N is the normal walking speed, set to 5 km/h for workers and visitors. This velocity represents the component which is inconsiderate of the robot-human interaction.

The reactive velocity of the human, $\vec{v_R}$, represents the human response to the alarm and consists of a proportional component and a derivative component. The proportional component is given by

$$\vec{v}_R^{(p)} = \lambda_p f_t \quad \text{where} \quad f_t = \frac{\vec{d}}{||\vec{d}||^2},$$

and $\vec{d}$ is the vector between the human and the robot. The derivative component adjusts the velocity based on the relative velocity to the robot, and is given by

$$\vec{v}_R^{(d)} = \lambda_d \frac{f_t - f_{t-1}}{\Delta_t}$$

where Δ_t is the time step. Finally, the reactive velocity can be expressed as

$$\vec{v_R} = \vec{v}_R^{(p)} + \vec{v}_R^{(d)} = \lambda_p f_t + \lambda_d \frac{f_t - f_{t-1}}{\Delta_t}, \tag{11}$$

where $\lambda_p = 1$ and $\lambda_d = 0.1$. If the alarm is inactive, the reactive velocity will be equal to zero. It can also be zero if the alarm is on, but the human does not react, which might be the case for some visitors.
The velocity resultant of the human, $\vec{v}$, is a combination of the nominal and reactive components, given by

$$\vec{v} = \frac{\vec{v_R} + \vec{v_N}}{\|\vec{v_R} + \vec{v_N}\|} \min\left(\|\vec{v_R} + \vec{v_N}\|, V_{\max}\right),$$

where $V_{\max} = \frac{13}{3.6}$ km/h is assumption of the maximum speed the human can reach. To ensure smooth transitions between the nominal and reactive behaviors at the distance $d = 10$, $\vec{v_R}$ should scale down as $d \to 10^-$ until becoming negligible for $d > 10$ compared to the nominal velocity. This scaling is achieved by using the logistic function

$$\text{scale}(d) = 1 - \frac{1}{1 + e^{-(\alpha d + \beta)}},$$

where $\alpha = 100$ controls the sharpness and $\beta = -\alpha d_{\text{critical}}$ the midpoint of the transition. Here, $d_{\text{active}} = 10$ implying that the reactive effect becomes attenuated as d transcends 10 m. The effect the parameters in terms of sharpness and active domain is illustrated in figure 9.

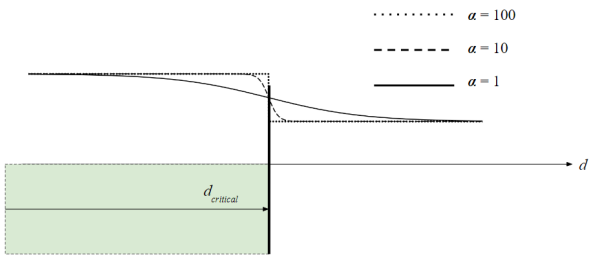

Figure 9: Diagram illustrating the activation function scale(d)

4 Results

The Monte Carlo simulation was conducted across a diverse range of scenarios, with each case comprising 100 iterations. The results are organized into two distinct sections: the first, *Pointwise Risk Analysis*, focuses on high-accuracy evaluations at specific points within the parameter space. The second, *Regional Risk Exploration*, employs broader exploration techniques to approximate risk surfaces and capture gradients across the parameter region.

4.1 Proposed Detection Systems

Table 4: Default Case Sensor Parameters

RGBD-CNN

Parameter	**Value**
P_u	0
P_f	0.0007
σ	0.02

RGBD-LiDAR

Parameter	**Value**
P_u	0
P_f	0.0006
σ	0.01

4.2 Pointwise Risk Analysis

Table 5: Risk Values for Sensor 1

# Workers	0 Visitors	1 Visitor	2 Visitors
1	0.11	0.35	0.51
2	0.31	0.86	0.87
3	0.57	0.86	0.97

Table 6: Risk Values for Sensor 2

# Workers	0 Visitors	1 Visitor	2 Visitors
1	0.13	0.22	0.48
2	0.26	0.53	0.85
3	0.48	0.81	0.94

As evident from the results the detection systems gave results indicating on injuries occurring with significant risk, for the case of 0 visitors, both sensors presented a risk in the order of ≈ 0.1 per loop. Assuming every loop is an i.i.d sample, the probability of at least one injury during the first k loops is.

$$\mathbb{P}(\text{At least 1 injury over k loops}) = 1 - 0.9^k \tag{12}$$

4.3 Regional Risk Exploration

Conducting high-accuracy simulations over a large domain can be time-consuming and computationally expensive. A more efficient approach to gain insights into potential system bottlenecks is to explore a larger, but sparsely sampled domain using fewer iterations combined with regression techniques. If the regression model demonstrates a good fit and performs well during evaluation, the results of this analysis can provide valuable guidance on how to effectively reduce risk, offering a strategic advantage by identifying critical areas for improvement with reduced computational effort.

A dataset containing 390 different results was obtained by grid search over ranges centered over the considered sensor parameter values. The number of iterations for each simulation was set to 10, emphasis was put on getting high resolution in the parameter space of interest.

Table 7: Parameter Ranges for Simulation

Parameter	**Min Value**	**Max Value**
P_u	0.000000	0.000222
P_f	0.000000	0.001000
σ	0.005	0.015
# Workers	1	2
# Visitors	0	2

Initially, evaluating the gradient of the RBF-kernel fitted to the data produced the following result for each sensor at the setting of 2 workers and 0 visitors, see figure 10 and 11.

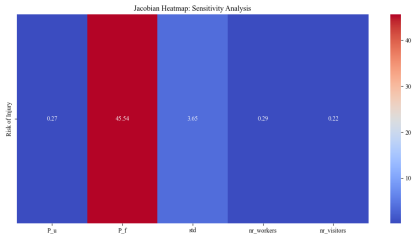

Figure 10: 2 Workers, 0 Visitors, RGBD-CNN

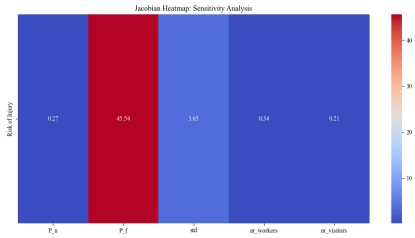

Figure 11: 2 Workers, 0 Visitors, RGBD-LiDAR.

The heat gradient maps show, that the result is very sensitive in terms of P_f. There is also a significant derivative in terms of the standard deviation σ, in the figure denoted "std". Plotting the risk-surface over P_f and σ for the case of 2 workers, 0 visitors. And the interpolated sensor, over n.o. workers and n.o. visitors produces the plots below. See figure 12 and figure 13

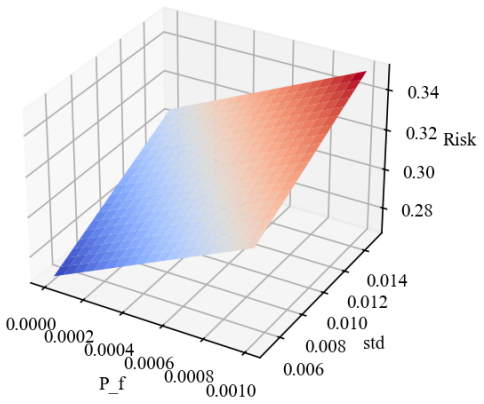

Figure 12: 2 Workers, 0 Visitors, $P_u = 0$

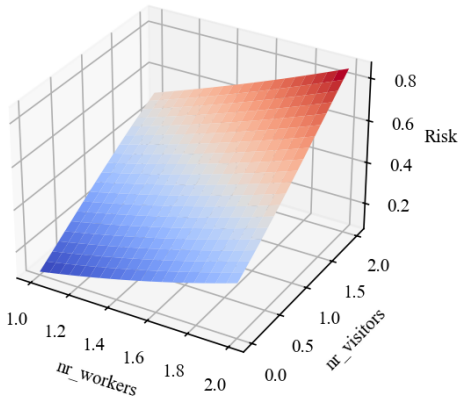

Figure 13: $P_u = 0$, $P_f = 0.00065$, $\sigma = 0.015$

5 Discussion

Discussion of Risk Analysis Results

Regional Risk Exploration

The results from both the regional risk exploration and pointwise risk analysis provide insights into the behavior of the detection systems under different scenarios. The simulation results indicate that among the primary drivers of injury risk is the failure of sensors P_f (false negatives). It is important however, to consider the difference in magnitude of the probability P_f in relation to the number of workers and visitors. This consideration indicates that the number of people might deserve equal attention.

In the regional risk exploration, it is observed that the gradient of the risk surface is substantial when P_f is increased. This underscores the high sensitivity of risk to the sensor's detection reliability. In scenarios where the number of workers is very low and there are no visitors, the overall risk might remain manageable. However, the introduction of visitors greatly amplifies the injury probability, particularly in cases of sensor failure. Visitors, who are less familiar with countermeasures, are especially vulnerable as they are modeled to react differently.

Pointwise Risk Analysis

The pointwise risk analysis further demonstrates the monotonic trend in terms of risk across various worker and visitor configurations. As shown in Tables 5 and 6, the presence of visitors leads to higher risk levels for both sensors. The RGBD-CNN sensor tends to perform slightly better in terms of lower risk values, but this is believed to be coincidental. Even so, the differences between sensors are overshadowed by the variability introduced by visitors, indicating that human factors and behavior, particularly those of untrained individuals, should be a primary concern when evaluating risk.

Population Density and Environmental Size

One of the critical insights emerging from the data is that the interaction intensity between individuals and the robot is not governed by population size alone, but by population density—the number of people relative to the size of the environment. Increasing the environment's size is believed to have a similar effect to decreasing the number of people in terms of risk reduction. Lower population density means fewer interactions between humans and the robot, which reduces the chances of undetected hazards. This suggests that future simulations should not only focus on modifying population numbers but also on adjusting the spatial configuration and size of the environment.

6 Conclusions

Given the assumptions of the environment and the human behaviors involved, as well as the two detection systems, it is concluded that the facility is not safe, as probabilities are in the order of 0.1 in the safest possible conditions which allow for productivity. The constraint in terms of space is very restrictive; scaling up the environment will decrease the spatial density of humans and, thus, it is believed that this will have an effect similar to simply removing people, as it is likely that population density, not the actual number of people in the environment, is the primary factor influencing risk.

Based on the discussion, the research questions can be briefly answered as follows:

1. Human presence: The number of people an especially visitors significantly impacts injury risk, emphasis on untrained individuals as they are more likely to be involved in accidents compared to trained workers.
2. Sensor failure probabilities (P_f): Higher probabilities of sensor failures lead to increased risk levels, emphasizing the importance of sensor reliability in detecting hazards.
3. Sensitivity parameters: Variations in the standard deviation (σ) directly influence the overall risk assessment and detection precision of the systems.

Given the two assumed detection systems, the greatest weakness seemed to lie in how the environment was setup. It is considered to small for safe and efficient operation of the robot. Thus, the first point is given extra emphasis as it seems to be the parameter with the "steepest gradient". s

Comments

The absorption probabilities were also successfully calculated; however, they were left out as they did not add meaningful results which fit into the scope of this particular study. It is, however, considered that the outlined method is still of value, as it provides a model of the internal behavior of the system, and not just a black box input-output relationship. Something that potentially allows for deeper analysis.

References

[1] Chiu, Ching-Te et al. "Chaos LiDAR Based RGB-D Face Classification System With Embedded CNN Accelerator on FPGAs". In: *IEEE Transactions on Circuits and Systems I: Regular Papers* 69.12 (2022), pp. 4847–4859. DOI: 10.1109/TCSI.2022.3190430.

[2] Corporation, Intel. *Intel RealSense Depth Camera D435*. https://www.intelrealsense.com/depth-camera-d435/. Accessed: 2024-10-01. 2024.

[3] Guevara, Leonardo et al. "Assessing the Probability of Human Injury During UV-C Treatment of Crops by Robots". In: *Proceedings of the Conference on Autonomous Systems*. University of Lincoln, UK, 2021.

[4] Life Sciences (NMBU), Norwegian University of. *Robotics Research Group*. Accessed: 2024-09-28. 2024. URL: https://www.nmbu.no/en/research/groups/robotics.

[5] Robotics, Saga. *The 2021 Light Treatment Season Has Started*. Accessed: 2024-09-28. 2021. URL: https://sagarobotics.com/the-2021-light-treatment-season-has-started/.

[6] Thrun, Sebastian, Burgard, Wolfram, and Fox, Dieter. *Probabilistic Robotics*. Cambridge, Massachusetts, London, England: MIT Press, 2006. ISBN: 978-0-262-20162-9.